INTERNATIONAL JOURNAL OF HYDROGEN ENERGY 39 (2014) 20560–20569

Available online at www.sciencedirect.com

ScienceDirect

journal homepage: www.elsevier.com/locate/he

Predicting radiative characteristics of hydrogen and hydrogen/methane jet fires using FireFOAM

C.J. Wang [a,c], J.X. Wen [b,*], Z.B. Chen [c], S. Dembele [c]

[a] State Key Laboratory of Fire Science, University of Science and Technology of China, Hefei, Anhui 230027, China
[b] Warwick FIRE, School of Engineering, University of Warwick, Coventry CV4 7AL, UK
[c] The Centre for Fire and Explosion Studies, Kingston University, London SW15 3DW, UK

ARTICLE INFO

Article history:
Received 30 December 2013
Received in revised form
4 April 2014
Accepted 7 April 2014
Available online 1 May 2014

Keywords:
Hydrogen jet fire
Hydrogen/methane jet fire
FireFOAM
Multi-component fuel

ABSTRACT

A possible consequence of pressurized hydrogen release is an under-expanded jet fire. Knowledge of the flame length, radiative heat flux as well as the effects of variations in ground reflectance is important for safety assessment. The present study applies an open source CFD code FireFOAM to study the radiation characteristics of hydrogen and hydrogen/methane jet fires. For combustion, the eddy dissipation concept for multi-component fuels recently developed by the authors in the large eddy simulation (LES) framework is used. The radiative heat is computed with the finite volume discrete ordinates model in conjunction with the weighted sum of grey gas model for the absorption/emission coefficient. The pseudo-diameter approach is used in which the corresponding parameters are calculated using the formulations of Birch et al. [24] with the thermodynamic properties corrected by the Able-Noble equation of state. The predicted flame length and radiant fraction are in good agreement with the measurements of Schefer et al. [2], Studer et al. [3] and Ekoto et al. [6]. In order to account for the effects of variation in ground surface reflectance, the emissivity of hydrogen flames was modified following Ekoto et al. [6]. Four cases with different ground reflectance are computed. The predictions show that the ground surface reflectance only has minor effect on the surface emissive power of the smaller hydrogen jet fire of Ekoto et al. [6]. The radiant fractions fluctuate from 0.168 to 0.176 close to the suggested value of 0.16 by Ekoto et al. [6] based on the analysis of their measurements.

Introduction

Hydrogen is regarded as an important clean energy carrier in the future energy landscape. However, safety issues related to pressurized hydrogen release are of concern and are being incorporated in the development of hydrogen safety Codes and Standards. A related particular hazard which needs to be addressed is hydrogen jet fires. If the pressure in storage tanks or transportation systems is more than 1.9 times the ambient pressure, the release is choked with the resulting jet being under-expanded and has sonic speed at the leak/rupture point. The resulting radiative jet fire extends to several metres and even more than ten metres. Direct impingement, convective or radiative heat from such jet fires can cause human casualties and damages to the directly affected and

* Corresponding author.
E-mail addresses: Jennifer.wen@warwick.ac.uk, j.wen@kingston.ac.uk (J.X. Wen).
http://dx.doi.org/10.1016/j.ijhydene.2014.04.062

surrounding equipment/facilities and in some severe cases can cascade to catastrophic consequences. There are only a handful of experimental facilities in the world wide scientific community which are able to test large scale hydrogen jet fires. Such full scale testing is extremely costly. In the mean time, it is also questionable to extrapolate the results from the limited conditions that can be tested. It is hence of considerable importance to develop and validate predictive tools which can quantify the flame and radiative characteristics of such under-expanded jet fires.

Several previous experimental studies [1–6] have focused on the radiative characteristics of under-expanded hydrogen jet fires, but relatively less computational fluid dynamics (CFD) efforts have been attempted. Brennan et al. [7] employed large eddy simulation (LES) approach to simulate hydrogen jet fires with laminar flamelet models and assumed PDF shape. They found that turbulence intensity only has limited effect on the flame length for which the predictions achieved reasonable agreement with the measurements. Houf et al. [8] also simulated hydrogen jet fires using Reynolds-averaged Navier–Stokes equations (RANS) and the eddy dissipation concept (EDC) model for combustion. Since subsonic inlet boundary conditions are specified at the pseudo-diameter, they found that the mesh size, turbulence model and turbulent intensity all influences the predictions of the flame length while similar to the findings of Brennan et al. [7], the effect of the turbulent intensity was found to be limited. The predicted flame length was also in reasonably good agreement with the measurements [2]. However, none of these numerical studies [7,8] addressed the radiative characteristics of under-expanded hydrogen jet fires.

The present study aims to validate the FireFOAM code, an LES solver based on open Source CFD toolbox OpenFOAM [9]. The development of FireFOAM [10] has been extensively supported by FM Global through internal effort as well as collaboration with worldwide institutions. FM Global also releases the developed models to the entire fire research community. The present study is part of effort to validate a recently modified EDC model for fuels with mixed components and radiative treatment for the predictions of hydrogen and hydrogen/methane jet fires. Particular attention is focused on the accurate predictions of radiative characteristics. The measurements from several published papers [2,3,6] including both hydrogen and hydrogen/methane jet fires are used for comparison as well as examination of the variation in ground reflectance.

Mathematical modelling

Governing equations

Hydrogen can be treated as an ideal gas at pressure lower than 172 bar [2]. The flow is governed by spatial filtering and Favre averaging of the reactive Navier–Stokes equations in the LES framework.

$$\frac{\partial \overline{\rho}}{\partial t}+\frac{\partial \overline{\rho}\tilde{u}_j}{\partial x_j}=0 \tag{1}$$

$$\frac{\partial \overline{\rho}\tilde{u}_j}{\partial t}+\frac{\partial \overline{\rho}\tilde{u}_i\tilde{u}_j}{\partial x_j}=\frac{\partial}{\partial x_j}\left(\overline{\rho}(\upsilon+\upsilon_t)\left(\frac{\partial \tilde{u}_i}{\partial x_j}+\frac{\partial \tilde{u}_j}{\partial x_i}-\frac{2}{3}\frac{\partial \tilde{u}_k}{\partial x_k}\delta_{ij}\right)\right)-\frac{\partial \overline{p}_d}{\partial x_i}-g_i x_i\frac{\partial \overline{\rho}}{\partial x_i} \tag{2}$$

$$\frac{\partial \overline{\rho}\tilde{h}_s}{\partial t}+\frac{\partial \overline{\rho}\tilde{u}_j\tilde{h}_s}{\partial x_j}=\frac{D\overline{p}}{Dt}+\frac{\partial}{\partial x_j}\left[\overline{\rho}\left(D+\frac{\upsilon_t}{Pr_t}\right)\frac{\partial \tilde{h}_s}{\partial x_j}\right]+\dot{q}'''-\nabla\cdot\dot{q}_r''' \tag{3}$$

$$\frac{\partial \overline{\rho}\tilde{Y}_m}{\partial t}+\frac{\partial \overline{\rho}\tilde{u}_j\tilde{Y}_m}{\partial x_j}=\frac{\partial}{\partial x_j}\left[\overline{\rho}\left(D+\frac{\upsilon_t}{Pr_t}\right)\frac{\partial \tilde{Y}_m}{\partial x_j}\right]+\overline{\omega}_m \tag{4}$$

$$\overline{p}=\overline{p}_d+\overline{\rho}g_j x_j \tag{5}$$

where ρ, u, p, h_s and Y are the density, velocity, pressure, sensible enthalpy and mass fraction of gas mixture, respectively. υ, υ_t, D, Pr_t denote laminar dynamic viscosity, turbulent dynamic viscosity, laminar diffusion coefficient and turbulent Prantl number. $\overline{\omega}_m$ is the production/sink rate due to gas reaction. $\dot{q}'''$ is the heat release rate per unit volume from a chemical reaction. $\dot{q}_r''$ is the sum of the radiative fluxes of all gas species, mainly water (H_2O) and carbon dioxide (CO_2).

The modified EDC combustion model

The eddy dissipation concept for the computation of turbulent combustion was originally proposed by Magnussen et al. [11,12] based on energy cascading. It assumes that turbulent mixing and combustion take place in fine structures (or smaller dissipative eddies) close to the Kolmogonov scale. The original EDC formulations were successful in RANS applications but various attempts [e.g. Refs. [13,14]] to extend it to LES had been problematic since the total kinetic energy required in the computation is not available and only the sub-grid scale (SGS) kinetic energy, which is a small part of the former, is resolved. This essentially requires the EDC model in the LES framework to be formulated with the SGS kinetic energy and eddy viscosity. Fureby et al. [13,14] directly replaced the total kinetic energy and its dissipation rate using SGS kinetic energy k_{SGS} and other SGS parameters. This approach has been adopted by some commercial CFD codes like FLUENT. However, it was reported that the predicted reaction rate is strongly dependent on grid size [13]. The problem was thought to be caused by the direct replacement of the total kinetic energy with the SGS kinetic energy, which is much smaller than the total kinetic energy and varies with the grid resolution.

Chen et al. [15] followed the energy cascade concept and derived the total kinetic energy and its dissipation rate using the SGS quantities as follows:

$$k=\left(\frac{3}{2C_{D1}^2}\right)^{1/3}(\varepsilon L')^{2/3} \tag{6}$$

$$\varepsilon=\sqrt{\frac{3}{2}}C_{D1}\frac{k_{SGS}^{3/2}}{\Delta}+\frac{2}{9}C_{D2}\upsilon\frac{k_{SGS}}{\Delta^2} \tag{7}$$

where $C_{D1}=0.135$ and $C_{D2}=0.5$. υ and Δ are the molecular kinetic viscosity and the filter size. k_{SGS} is obtained together with SGS ε_{SGS} and υ_t by using the one-equation LES model of Menon et al. [16] to close the above governing equations. The

integral length scale L' is evaluated as the characteristic plume length of the fire following the wide practice of the fire research community [17]:

$$L\prime = \left(\frac{Q}{\rho_\infty C_p T_\infty \sqrt{g}}\right)^{2/5} \tag{8}$$

where Q is the heat release rate, kW; ρ_∞, C_p, T_∞ and g are the ambient density, specific heat at constant pressure, temperature and the acceleration of gravity, respectively.

Thus the characteristic length L^* and velocity scale u^* of the fine structure can be written as

$$L^* = \frac{2}{3}\left(\frac{3C_{D2}^3}{C_{D1}^2}\right)^{1/4}\left(\frac{\upsilon^3}{\varepsilon}\right)^{1/4} \tag{9}$$

$$u^* = \left(\frac{C_{D2}}{3C_{D1}^2}\right)^{1/4}(\upsilon\varepsilon)^{1/4} \tag{10}$$

The reaction mechanism and rate

The above modified EDC has been further extended by the present authors to account for the combustion of fuels with mixed components using either infinitely-fast chemistry or finite rate chemistry. For the present study, infinitely-fast chemistry is assumed for hydrogen or hydrogen/methane as follows:

$$H_2 + 0.5O_2 \rightarrow H_2O \tag{11}$$

$$CH_4 + 2O_2 \rightarrow CO_2 + 2H_2O \tag{12}$$

If only hydrogen is involved, eq. (11) is chosen.

The essence of the EDC is that chemical reactions take place in the fine structures. It is further assumed that the fine structures can be described as stationary homogeneous Perfectly Stirred Reactors (PSR). Thus in each computational cell, the remaining reactants and newly formed products in the fine structure mix with the surrounding fluids through turbulent diffusion. The filtered reaction rate for the species mass-fraction transport equation can be expressed as:

$$\overline{\omega}_i = \overline{\rho}\dot{m}^*\frac{\gamma\chi}{1-\gamma\chi}\left(\tilde{Y}_i - Y_i^*\right) \tag{13}$$

where $\overline{\rho}$, γ, χ and $\tilde{Y}_i$ are the filtered density, mass fraction of the fine structures, reacting fraction of the fine structures and mean species mass fraction. The species mass fraction in fine structures Y_i^* are evaluated for the above infinitely-fast reactions as

For fuels:

$$Y_{f,i}^* = \tilde{Y}_{f,i} - \left(\frac{\tilde{Y}_{f,i}}{\sum_{j=1}^{N_F}\frac{\tilde{Y}_{f,j}}{\mathrm{abs}\left(\sum_{n=1}^{NR}\upsilon'_{f,j,n}\cdot W_{f,j}\right)}}\right) \times \min\left(\sum_{j=1}^{N_F}\frac{\tilde{Y}_{f,j}}{\mathrm{abs}\left(\sum_{n=1}^{NR}\upsilon'_{f,j,n}\cdot W_{f,j}\right)}, \frac{\tilde{Y}_{O_2}}{\mathrm{abs}\left(\sum_{n=1}^{NR}\upsilon'_{O_2,n}\cdot W_{O_2}\right)}\right) \tag{14}$$

For oxidizer O_2:

$$Y_{O_2}^* = \tilde{Y}_{O_2} - \mathrm{abs}\left(\sum_{n=1}^{NR}\upsilon'_{O_2,n}\cdot W_{O_2}\right) \cdot \min\left(\sum_{j=1}^{N_F}\frac{\tilde{Y}_{f,j}}{\mathrm{abs}\left(\sum_{n=1}^{NR}\upsilon'_{f,j,n}\cdot W_{f,j}\right)}, \frac{\tilde{Y}_{O_2}}{\mathrm{abs}\left(\sum_{n=1}^{NR}\upsilon'_{O_2,n}\cdot W_{O_2}\right)}\right) \tag{15}$$

For products (CO_2 and H_2O):

$$Y_{p,i}^* = \tilde{Y}_{p,i} + \mathrm{abs}\left(\sum_{n=1}^{NR}\upsilon'_{p,i,n}\cdot W_{p,i}\right) \cdot \min\left(\sum_{j=1}^{N_F}\frac{\tilde{Y}_{f,j}}{\mathrm{abs}\left(\sum_{n=1}^{NR}\upsilon'_{f,j,n}\cdot W_{f,j}\right)}, \frac{\tilde{Y}_{O_2}}{\mathrm{abs}\left(\sum_{n=1}^{NR}\upsilon'_{O_2,n}\cdot W_{O_2}\right)}\right) \tag{16}$$

where NR, N_F, υ' and W_j are reaction number, fuel number, stoichiometric coefficients and species molecular weight, respectively. The term "abs( )" is a function used to return the absolute value of its parameter.

The mass transfer rate between the fine structures and the surrounding fluids $\dot{m}^*$ can be calculated as

$$\dot{m}^* = \frac{2u^*}{L^*} = \left(\frac{3}{C_{D2}}\right)^{1/2}\left(\frac{\varepsilon}{\upsilon}\right)^{1/2} \tag{17}$$

Following Magnussen [18], the mass fraction of the fine structures might be written as

$$\gamma = \left(\frac{L^*}{L'}\right)^{\alpha} \tag{18}$$

where $\alpha = 0.2$.

Chen et al. [15] suggested that the reacting fraction of the fine structures is expressed as

$$\chi \approx \begin{cases} \dfrac{Z}{Z_{st}} & \text{if } 0 \le Z < Z_{st} \\ \dfrac{1-Z}{1-Z_{st}} & \text{if } Z_{st} < Z \le 1 \end{cases} \tag{19}$$

In eq. (19), following Bilger's definition [19], one can obtain

$$Z = \frac{\left(\frac{2Y_C}{W_C} + \frac{Y_H}{2W_H}\right)_F + \frac{Y_O^\infty}{W_O}}{\left(\frac{2Y_C^I}{W_C} + \frac{Y_H^I}{2W_H}\right)_F + \frac{Y_O^\infty}{W_O}} \tag{20}$$

$$Z_{st} = \frac{\frac{Y_O^\infty}{W_O}}{\left(\frac{2Y_C^I}{W_C} + \frac{Y_H^I}{2W_H}\right)_F + \frac{Y_O^\infty}{W_O}} \tag{21}$$

where Y_k and W_k are the elemental mass fraction and atomic weight for element k; Superscript I and ∞ refer to values at the inlet and ambient condition, respectively; Subscript F denotes fuel stream.

Radiation model

It is common to consider laboratory-scale hydrogen or hydrogen/methane flames as optically thin. This may not be necessarily true for large scale hydrogen jet fires. The optical

thickness κ can be approximated as $a_p \times S$ [20], where a_p is Planck mean absorption coefficient and S is a characteristic length, equal to $W_f/2$. $\kappa << 1$ corresponds to optically thin flame while $\kappa >> 1$ shows the flame is optically thick. A value of 1 m implies a self-absorbing medium. For the jet fires of Schefer et al. [2], Studer et al. [3] and Ekoto et al. [6], the optical thickness is estimated to be 0.8, 1.2 and 2.1 respectively. This means these jet fires cannot be regarded as optical thin. They fall close to be a self-absorbing medium, i.e. radiation absorption occurs within the fire.

The finite volume discrete ordinates model (fvDOM) is used to solve the radiative heat transfer equation. CO_2 and H_2O are main contributors to flame radiation. Strictly speaking this requires the radiative transport equations to be resolved over all spectral bands of CO_2 and H_2O. But this will be computationally costly. As an alternative, the weighted sum of grey gas model [21,22] is used to evaluate the absorption/emission coefficient. This model is regarded as a reasonable compromise between the oversimplified grey gas model and a narrow band type models which take into account particular absorption bands.

Numerical methods

Within OpenFOAM toolbox [9], the governing equations are discretized using the finite volume technique on a non-uniform grid. The time derivative is discretized using the backward time scheme with second order accuracy, and the central differencing scheme with second order accuracy is used to discretize both the diffusion and gradient terms. The Gauss limited linear differencing scheme is employed to evaluate the convection term in order to maintain the total variation diminishing (TVD) characteristic. For the source term, the implicit scheme is adopted. Additionally, for both the inner and outer loop iterations at every time step, the PIMPLE algorithm, which is a combination of pressure implicit with splitting of operators (PISO) and semi-implicit methods for pressure-linked equations (SIMPLE), is used to update the field variables.

Numerical set up

For model validation, three typical experimental cases, as shown in Table 1, have been simulated. Additional parametric studies have also been carried out for further three cases (4–6) to investigate the ground reflection effect on radiative parameters.

Following the pseudo-source approach, the parameters at the jet exit can be calculated following isentropic expansion relations from stagnation conditions in the tank to the sonic condition at the jet exit. From a CFD perspective, a pseudo-diameter would be better at which the jet pressure has equilibrated with the ambient conditions. Birch et al. [23] firstly proposed a pseudo-diameter formulation based on experimental findings. Their formulation considers the area which would be occupied by the same mass flow rate at ambient pressure and temperature with a sonic speed. Subsequently, Birch et al. [24] derived an alternative definition that conserves both mass and momentum though the expansion zone while retaining the assumption that the pressure is reduced to the ambient level and the temperature is equal to that in the tank at the position of the pseudo-source. Another alternative method is Mach disk analysis that can yield the subsonic condition at pseudo-diameter [25]. This analysis assumes an isentropic expansion from the jet exit to the place just upstream of the Mach disk, followed by normal shock relations of Mach disk. Thus the Mach disk diameter becomes pseudo-diameter while the velocity and temperature behind the Mach disk with ambient pressure becomes inlet parameters. The later subsonic inlet conditions are more favourable for the present cases but were found to result in 50% over-prediction of the flame length in comparison with the measurements. Hence, the thermodynamic

Table 1 – Operating conditions of the six cases computed.

Case		1	2	3[a]	4	5	6
Jet direction (H – horizontal; V – vertical)		V	H	H	H	H	H
Nozzle diameter (mm)		5.08	10	20.9	20.9	20.9	20.9
Tank pressure (bar)		104.8	32.99	59.8	59.8	59.8	59.8
Tank temperature (K)		231.4	276.01	308.7	308.7	308.7	308.7
Fuel		H_2	Hydrogen/methane (80%:20%)	H_2	H_2	H_2	H_2
Ambient temperature (K)		293	283.15	280	280	280	280
Ambient pressure (bar)		1.0	1.0	1.022	1.022	1.022	1.022
Wind speed		0	0	2.84	2.84	2.84	2.84
Angle between wind and jet directions (°)		0	0	1.5	1.5	1.5	1.5
Ground reflectance		0	0	0.5	0.0	0.8	0.2
Pseudo conditions	Diameter (mm)	31.5	35.0	97.9	97.9	97.9	97.9
	Velocity (m/s)	1795	1252.4	2061	2061	2061	2061
	Temperature (K)	231.4	276	308.7	308.7	308.7	308.7
	Pressure	1.0	1.0	1.022	1.022	1.022	1.022
Experimental data		Schefer et al. [2]	Studer et al. [3]	Ekoto et al. [6]	–	–	–

[a] Among the two jet fires tested by Ekoto [6], the smaller one was simulated in the present study so that a reasonably find grid resolution of 1 mm across the pseudo-diameter within the time scale required to complete the work.

properties required in calculating the pseudo-diameters given by Birch et al. [24] were modified by using the Able-Noble equation of state [2] for all the six cases listed in Table 1. In case 1, the hydrogen enters the domain through a nozzle with the pseudo-diameter of 31.5 mm and inlet velocity of 1795 m/s at 231.4 K and 1.0 atm. In case 2, the nozzle inlet has a pseudo-diameter of 35.0 mm with inlet velocity of 1252.4 m/s, temperature of 276 K and ambient pressure of 1.0 atm. For cases 3–6, the inlet parameters include pseudo-diameter at 97.9 mm, velocity at 2061 m/s, temperature at 308.7 K and the pressure at 1.022 atm.

Open boundaries are imposed on all the surfaces except hydrogen or hydrogen/methane inlet and bottom ground surface in cases 3–6. While the other conditions remain the same, the ground surface in cases 3–6 has different reflectance values. It should be noted that, in Ekoto et al.'s experiments [6], an approximate 25 m by 15 m concrete pad was set in front of the release location and covered with steel sheet directly beneath the release path. Thus current ground surface with the size of 25 m × 10 m is smaller than the steer sheet and can be approximately defined as the whole one with only one reflectance. Additionally, to simplify the mesh and numerical set up, a uniform wind surface was imposed at the inlet for cases 3–6 by ignoring the angle of 1.5° between the wind and jet inlet. Non-uniform meshes are used with grid points clustered around the inlet centre and their sizes gradually increased in the radial and vertical direction.

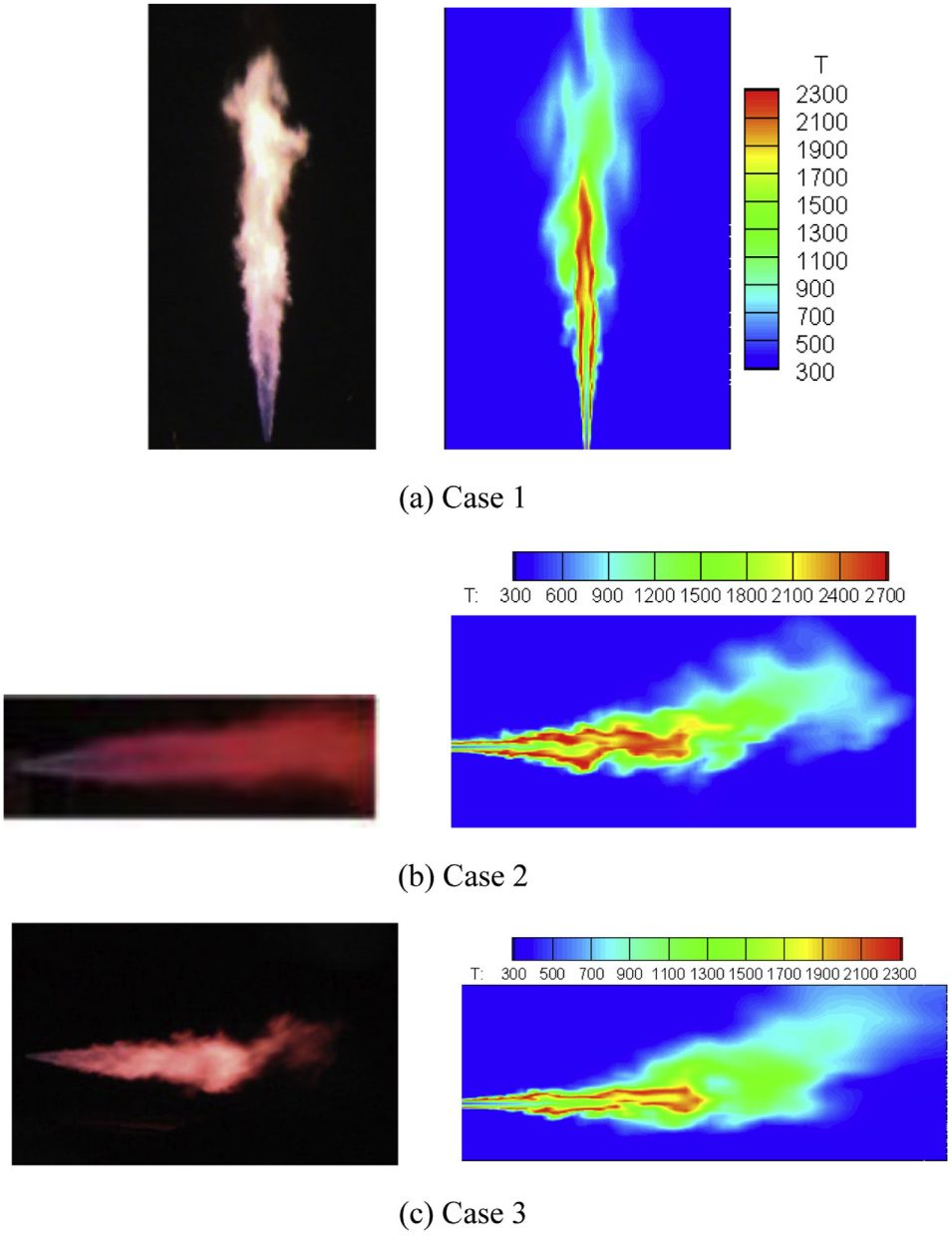

Fig. 1 – The measured (left) and predicted (right) flame shapes for all three cases considered. Note that the measured images come from the references [2,3,6].

Results and discussions

Taking into account the availability of measurements, the predictions were compared with the experimental data for flame shape, flame height, radiant fraction and surface emissive power.

Flame shape

The measured and predicted flame envelopes are shown for all three cases in Fig. 1. In the experiments, the flame envelopes were measured by visible cameras in Refs. [2,3] and thermal imaging infrared cameras in Refs. [3,6]. The predicted flame shapes are represented using shaded temperature contours. It should be noted that the measured images were not scaled [2,3,6] and hence the predicted and measure flame shapes presented in Fig. 1 are not necessarily in the same scale. However, the similarities between them are evident.

Flame length

For comparison, the visible flame length L_{vis} was calculated following Schefer et al. [2] as follows:

$$L_{vis} = \frac{L^* d_{sd}\sqrt{\rho_{sd}/\rho_\infty}}{f_s} \tag{23}$$

In the buoyancy dominated regime (flame Froude number $Fr_f < 5$), the non-dimenstional flame length L^* is expressed as

$$L^* = \frac{13.5 Fr_f^{2/5}}{\left(1 + 0.07 Fr_f^2\right)^{1/5}} \tag{24}$$

and in the momentum-dominated regime:

$$L^* = 23 \tag{25}$$

$$Fr_f = \frac{u_{sd} f_s^{3/2}}{(\rho_{sd}/\rho_\infty)^{1/4}[((T_{ad} - T_\infty)/T_\infty) g d_{sd}]^{1/2}} \tag{26}$$

where subscript sd denotes jet exit; f_s and T_{ad} are the mass fraction of fuel at stoichiometric conditions and adiabatic flame temperature, respectively.

In post-processing the current predictions, the transient flame length is determined by $L = \max(\hat{x}\cdot\hat{I}_g)\big|_{\hat{Y}_{ref}\geq 0}$, where $\hat{x}$, $\hat{I}_g$ and $\hat{Y}_{ref} = \hat{Y}_{Fuel} - \hat{Y}_{O_2}/s$ are cell-centre coordinate vector, unit vector of jet direction and reference specie mass fraction, respectively. Fig. 2 shows flame lengths for cases 1–3. The transient flame lengths fluctuate due to pulsation of the fire. The mean flame length can be defined depending on the intermittency following Zukoski et al. [26]. The intermittent rate of 0.5 for the mean flame length is chosen as the hydrogen jet fire is in pseudo-steady state. Table 2 shows the comparison between the predicted mean flame length, the measured visible flame length and the flame lengths calculated by some empirical correlations. In all three cases, there is reasonably good agreement between the predicted, measured flame lengths as well as the theoretical values. The largest discrepancy is found in case 2 for the H_2/CH_4 blended fuel, the

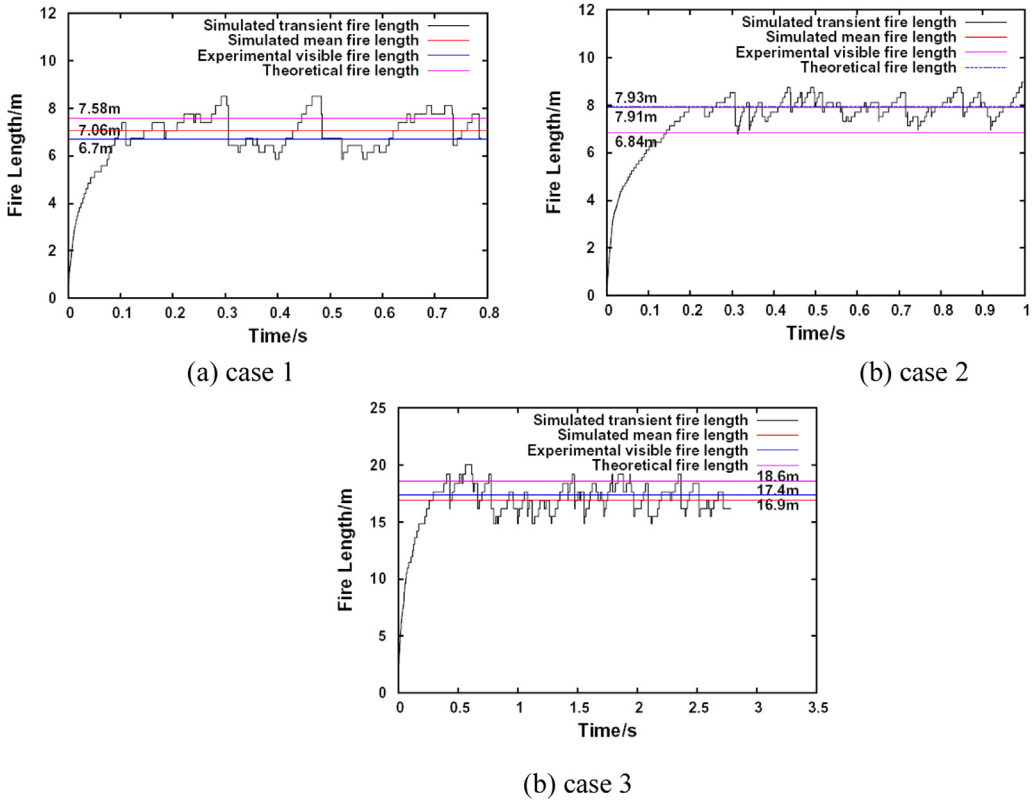

Fig. 2 – Comparison of the predicted and measured flame length.

Table 2 – Comparison between the predicted, measured and empirically evaluated flame lengths.

Case	Predicted (m)	Measured (m)	Theoretical (m)	Discrepancy between the predicted and measured values	Discrepancy between the numerical predictions and theoretical values
1	7.06	6.7	7.58	+5.4%	−6.9%
2	7.91	6.84	7.93	+15.6%	−0.25%
3	16.9	17.4	18.6	−2.9%	−9.1%

discrepancy between the predicted and measured flame length is 15.6% while the predicted flame length is only 0.25% different from the theoretical value of 7.93 m. Studer et al. [3] also found that the measured flame length departs evidently from the theoretical value, which seems to be attributed to gas mixture, especially methane added to hydrogen.

Radiant fraction

Turns and Myhr [27] proposed that the flame radiant fraction R_r correlates well with the flame residence time τ_f for a wide variety of fuels and defined the later as

$$\tau_f = \frac{\rho_f W_f^2 L_{vis} f_s}{3\rho_{sd} d_{sd}^2 u_{sd}} \tag{27}$$

where flame width W_f is approximately equal 0.17 L_{vis} and ρ_f is flame density given by $p_{amb}M_f/(RuT_{ad})$ (p_{amb} is the ambient pressure, M_f is the stoichiometric fuel/air molecular weight, and Ru is the universal gas constant).

Molina et al. [28] further showed that radiant fraction is proportional to a factor related to the resident time τ_f multiplied by $a_p T_{ad}^4$. Following this correlation, Studer et al. [3] proposed an expression for theoretically predicting radiant fraction of hydrogen/methane jet fires in case 2:

$$R_r = 0.08 \log_{10}(\tau_f a_p T_{ad}^4) - 1.14 \tag{28}$$

while Ekoto et al. [6] developed another one for hydrogen jet fires as shown in case 3 as

$$R_r = 0.08916 \log_{10}(\tau_f a_p T_{ad}^4) - 1.2172 \tag{29}$$

In the simulation, the radiant fraction over the whole flame (R_r) is calculated from

$$R_r = \left. \frac{\sum_{cell} (\nabla \cdot q_r')_{cell} dV_{cell}}{\sum_{cell} (\overline{\omega}_{fu} \Delta h_c)_{cell} dV_{cell}} \right|_{\widehat{Y}_{ref} \geq 0} \tag{30}$$

where V, $\overline{\omega}_{fu}$ and Δh_c are cell volume, fuel sink rate and chemical enthalpy, respectively. This approach does not need to assume flame shape.

Fig. 3 and Table 3 show the comparison between the predicted, experimental and theoretically evaluated radiant fraction. For case 1, there was no published experimental data

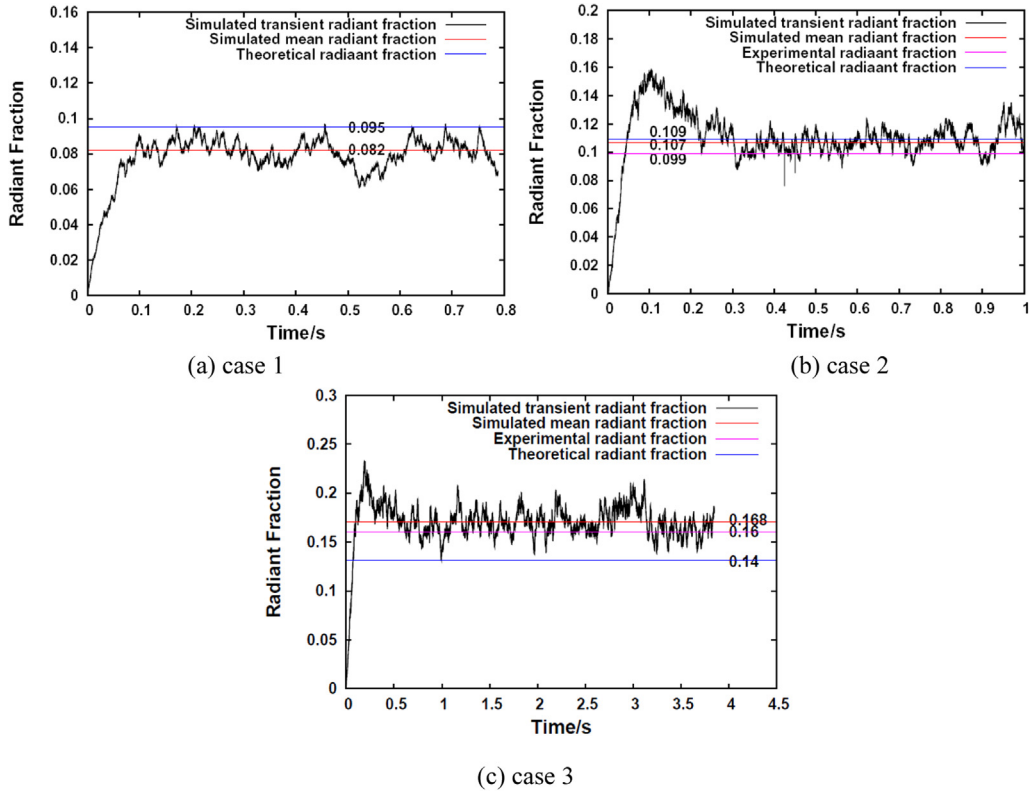

Fig. 3 – Predicted radiant fraction.

Table 3 – Comparison between the predicted, experimental and theoretically evaluated radiant fraction.

Case	Predicted	Experimental	Theoretical	Discrepancy between the predicted and measured values	Discrepancy between the numerical predictions and theoretical values
1	0.082	–	0.095	–	−13.7%
2	0.107	0.099	0.109	+8.1%	−1.8%
3	0.168	0.16	0.14	+5.0%	+20.0%

for comparison in reference of Schefer et al.'s [2]. The predicted mean radiant fraction is 0.082, 13.7% different from the theoretically calculated value. For case 2, the mean radiant fraction overpredicts the experimental data by 8.1% and underpredicts the theoretical value by only 1.8%. It should be noted that this experimental value is evaluated by using the measured radiative heat flux at radiometer 5 (4 m from the jet centreline) [3] and a non-dimensional radiant power term, $C^* = 0.85$ suggested by Sivathanu and Gore [29]. For case 3, the mean radiant fraction is 0.168. The relatively larger value in comparison with cases 1 and 2 can possibly be attributed to the larger jet diameter, which results in larger flame width and length as well as stronger ground reflection of the incident radiation, etc. Ekoto et al. [6] measured the radiative fluxes at different positions in the jet fire, and calculated the radiant fraction as 0.22 by single point source method and 0.16 by the weighted multi source model. They suggested that the latter value is a closer representation of the practical situations. In this regard, the present prediction is in very good agreement with the estimated value of Ekoto et al. from their experiments [6]. A relatively large discrepancy of 20% is found between the numerically predicted and theoretical values. This can possibly be attributed to the ignorance of ground reflection effect in the theoretical calculation.

Effects of variations in ground reflectance

In the experiment setting for case 3, there was a concrete pad covered with steel sheeting underneath the horizontal jet fire. The steel sheeting has an infrared surface reflectance of 0.5. Ekoto et al. [6] found that the amount reflected was dependant on the relative orientation and location of the radiometer, steel/concrete surfaces, the jet flame and the overall surface condition. The recorded heat fluxes were found to increase by up to 50% for certain configurations. To further investigate the effects of ground surface reflectance on flame radiant fraction, numerical experiments are conducted for a further three cases with ground surface reflectance values of 0, 0.2, and 0.8 while the other conditions are kept the same as case 3.

Fig. 4 presents the predicted mean surface emissive power against the ground surface reflectance. It is found that the ground surface reflectance has a minor effect on the surface emissive power of the jet fire. This should be thought to be caused by the jet fire infrared irradiance being partially reflected back to the fire by steel sheeting. The increased ground surface reflectance promotes temperature and surface emissive power of the lower flame part. The corresponding gas flame density and buoyancy increase in the vertical direction or radial direction of the flame, which leads to the wider flame in the vertical direction and gives negative feedback to the temperature increase. So there seems to be competition of temperature increase by larger reflected heat flux and its decrease by the resultant lower density, which determines the increase or decrease the surface emissive power. In other word, the increase of ground reflectance does not result in a linear increase in the surface emissive power. Furthermore, the jet centreline is 3.25 m above the ground surface. The relatively small inlet and reflected radiative heat fluxes on the ground surface have little effect on the jet fire. The surface emissive power of hydrogen jet fire is found to be between 33.4 kW/m^2 and 33.7 kW/m^2 and its variation is within 0.9%. However, at the near-field radiometer locations, the reflected radiative heat flux possibly has a comparable value with the one from the jet fire. So in experiments [6], the reflective addition to the radiometer was found to be high, and up to 50%.

The relationship between radiant fraction R_r and surface emissive power SEP can be expressed as

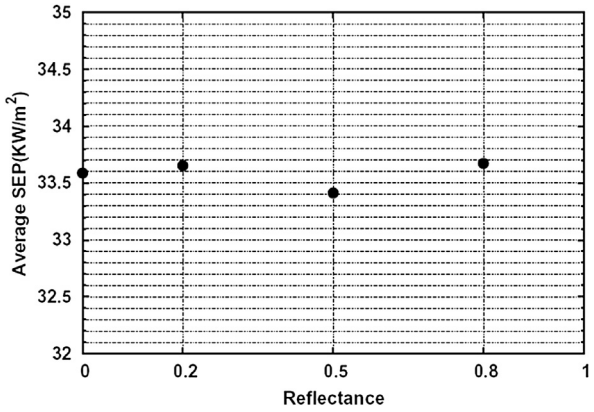

Fig. 4 – The predicted mean surface emissive power *vs* ground surface reflectance.

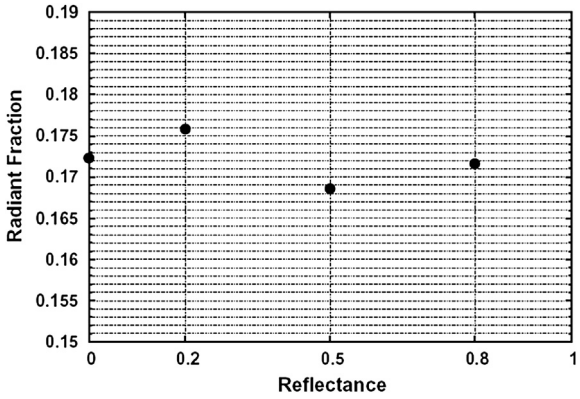

Fig. 5 – The predicted mean radiant fraction *vs* ground surface reflectance.

$$R_r = \frac{SEP \cdot A_f}{Q} \quad (31)$$

where A_f and Q are fire surface area and total fire heat release rate. Normally, Q is constant for a given fire. The radiant fraction hence changes with the SEP as A_f is kept almost constant. This is further illustrated in Fig. 5, where the radiant fraction has similar trend as the surface emissive power and ranges from 0.168 to 0.176. The discrepancy is about 5%, much larger than that of surface emissive power. That is, the radiant fraction exhibits more sensitive to the ground surface reflectance.

Conclusions

Six cases of under-expanded hydrogen and hydrogen/methane jet fires are simulated using open source CFD code FireFOAM in the LES frame. Combustion and radiative heat transfer are computed using the eddy dissipation concept for multi-component fuels recently developed by the authors and the finite volume discrete ordinates model. The predictions are found to be in very good quantitative agreement for flame length and radiant fraction with the measurements of Schefer et al. [2], Studer et al. [3] and Ekoto et al. [6]. These results have demonstrated that the FireFOAM code can be used as a reliable predictive tool for hazard analysis of hydrogen and hydrogen/methane jet fires.

In order to investigate the effects of ground surface reflectance on the radiant fraction, four cases with different ground surface reflectance are simulated with one having the same as the experimental condition of Ekoto et al. [6]. The predictions show that the ground surface reflectance only has minor effect on the surface emissive power of the jet fire. The radiant fractions fluctuate from 0.168 to 0.176 close to the suggested value of 0.16 by Ekoto et al. [6] based on the analysis of their measurements. Moreover, they seem are more sensitive to the ground surface reflectance than surface emissive power. The increase of ground surface reflectance does not result in a linear increase in the surface emissive power and the radiant fraction.

Acknowledgement

The authors would like to acknowledge the funding from the European Commission FP7-IIF Project (Grant No. 909658), the National Natural Science Foundation of China (Grant No. 51276177), the National Basic Research Program of China (973 Program, Grant No. 2012CB719704) and the Fundamental Research Funds for the Central Universities.

We are grateful to Etienne Studer, from the Heat Transfer and Fluid Mechanics Laboratory, France, for providing details of their hydrogen/methane jet fire measurements.

REFERENCES

[1] Schefer RW, Houf WG, Bourne B, Colton J. Spatial and radiative properties of and open-flame hydrogen plume. Int J Hydrogen Energy 2006;31:1332–40.

[2] Schefer RW, Houf WG, Williams TC, Bourne B, Colton J. Characterization of high-pressure, underexpanded hydrogen-jet flames. Int J Hydrogen Energy 2007;32:2081–93.

[3] Studer E, Jamois D, Jallais S, Leroy G, Hebrard J, Blanchetière V. Properties of large-scale methane/hydrogen jet fires. Int J Hydrogen Energy 2009;34:9611–9.

[4] Lowesmith BJ, Hankinson G. Large scale high pressure jet fires involving natural gas and natural gas/hydrogen mixtures. Process Saf Environ Prot 2012;90:108–20.

[5] LowesMith BJ, Hankinson G. Large scale experiments to study fires following the rupture of high pressure pipelines conveying natural gas and natural gas/hydrogen mixtures. Process Saf Environ Prot 2013;91:101–11.

[6] Ekoto IW, Houf WG, Ruggles AJ, Creitz LW, Li JX. Large-scale hydrogen jet flame radiant fraction measurements and modelling. In: Proceedings of the 2012 9th the international pipeline conference, Calgary, Alberta, Canada, 2012, Paper IPC2012–90535; 2012.

[7] Brennan SL, Makarov DV, Molkov V. LES of high pressure hydrogen jet fire. J Loss Prev Process Indust 2009;22:353–9.

[8] Houf WG, Evans GH, Schefer RW. Analysis of jet flames and unignited jets from unintended releases of hydrogen. Int J Hydrogen Energy 2009;34:5961–9.

[9] OpenFOAM users' guide. Available from: http://www.opencfd.co.uk/openfoam/.

[10] Wang Y, Chatterjee P, de Ris JL. Large eddy simulation of fire plumes. Proc Combust Inst 2011;33:2473–80.

[11] Magnussen BF, Hjertager B. On mathematical modeling of turbulent combustion with special emphasis on soot formation and combustion. In: 16th Symp. (Int.) on Combustion. Pittsburgh, PA: The Combustion Inst.; 1976. pp. 719–29.

[12] Magnussen BF, Hjertager BH, Olsen JG, Bhaduri D. Effects of turbulent structure and local concentrations on soot formation and combustion in C_2H_2 diffusion flames. In: 17th Symp. (Int.) on Combustion. Pittsburgh, PA: The Combustion Inst.; 1978. pp. 1383–93.

[13] Fureby C, Löfström C. Large-eddy simulations of bluff body stabilized flames. In: 25th Symp. (Int.) on Combustion. Pittsburgh, PA: The Combustion Inst.; 1994. pp. 1257–64.

[14] Möller SI, Lundgren E, Fureby C. Large eddy simulation of unsteady combustion. In: 26th Symp. (Int.) on Combustion. Pittsburgh, PA: The Combustion Inst.; 1996. pp. 241–8.

[15] Chen Z, Wen JX, Xu BP, Dembele S. Large eddy simulation of fire dynamics with the improved eddy dissipation concept. In: 10th IAFSS symposium. USA: University of Maryland; June 19–24, 2011.

[16] Menon S, Yeung PK, Kim WW. Effect of subgrid models on the computed interscale energy transfer in isotropic turbulence. Comput Fluids 1996;25:165–80.

[17] Baum H, McGrattan K, Rehm R. Three dimensional simulations of fire plume dynamics, fire safety science. In: Proceedings of the fifth international symposium, Melbourne, Australia; 1997. pp. 511–22.

[18] Magnussen BF. The eddy dissipation concept: a bridge between science and technology. In: Thematic conference on computational combustion, Lisbon, Portugal; 2005. pp. 1–25.

[19] Bilger RW, Starner SH, Kee RJ. On reduced mechanisms for methane–air combustion in non-premixed flames. Combust Flame 1990;80(2):135–49.

[20] Siegel R, Howell JR. Thermal radiation heat transfer. New York: Hemisphere Publishing Corporation; 1981. p. 862.

[21] Smith TF, Shen ZF, Friedman JN. Evaluation of coefficients for the weighted sum of gray gases model. J Heat Transf 1982;104:602–8.

[22] Coppalle A, Vervisch P. The total emissivities of high-temperature flames. Combust Flame 1983;49:101–8.

[23] Birch AD, Brown DR, Dodson MG, Swaffield F. The structure and concentration decay of high pressure jets of natural gas. Combust Sci Technol 1984;36:249–61.
[24] Birch AD, Hughes DJ, Swaffield F. Velocity decay of high pressure jets. Combust Sci Technol 1987;52:161–71.
[25] Winters WS, Evans GH. Final report for the ASC gas-powder two-phase flow modeling, Project AD2006–AD2009, Sandia National Laboratories Report no. SAND2006-7579.
[26] Zukoski EE, Cetegen BM, Kubota T. Visible structure of buoyant diffusion flames. In: 20th Symp. (Int.) on Combustion. Pittsburgh, PA: The Combustion Inst.; 1984. pp. 361–6.
[27] Turns SR, Myhr FH. Oxides of nitrogen emissions from turbulent jet flames: part I – fuel effects and flame radiation. Combust Flame 1991;87:319–35.
[28] Molina A, Schefer RW, Houf WG. Radiative fraction and optical thickness in large-scale hydrogen-jet fires. Proc Combust Instute 2006;31:2565–73.
[29] Sivathanu YR, Gore JP. Total radiative heat-loss in jet flames from single-point radiative flux measurements. Combust Flame 1993;94:265–70.